Super High-Frequency Scandium Aluminum Nitride Crystalline Film Bulk Acoustic Resonators

Mingyo Park
Department of Electrical and Computer Engineering
Georgia Institute of Technology
Atlanta, GA, USA
m.park@gatech.edu

Jialin Wang
Department of Electrical and Computer Engineering
Georgia Institute of Technology
Atlanta, GA, USA
jwang462@gatech.edu

Rytis Dargis
IQE Plc
Greensboro, NC, USA
RDargis@iqep.com

Andrew Clark
IQE Plc
Greensboro, NC, USA
AClark@iqep.com

Azadeh Ansari
Department of Electrical and Computer Engineering
Georgia Institute of Technology
Atlanta, Ga, USA
azadeh.ansari@ece.gatech.edu

***Abstract*—This work presents promising results of overtone thickness resonance modes of film bulk acoustic resonators (FBARs) operating at K_u band, traditionally perceived unachievable by acoustic devices. We take advantage of the epitaxial growth of the bottom metal electrode, as well as the piezoelectric layer to improve thin-film crystal quality and hence quality factor (*Q*). This work is the first demonstration of a multi-GHz FBAR realized on single-crystalline $Sc_{0.12}Al_{0.88}N$/Mo stack.**

Keywords—5G mobile communication, Films bulk acoustic resonators, Acoustic filters, Single crystalline, Scandium aluminum nitride, Epitaxial molybdenum, Molecular beam epitaxy.

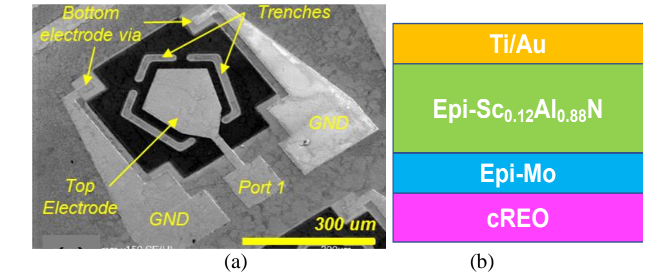

(a) (b)

Fig.1. (a) SEM imag of the fabricated $Sc_{0.12}Al_{0.88}N$ apodized FBAR. (b) Resonant stack with a total stack tickness of ~550 nm.

I. Introduction

Emerging next-generation wireless communication devices call for high-performance filters that operate at 3-30 GHz (super-high frequency range) and offer low loss, wide bandwidth and steep skirts [1]. The thin films bulk acoustic resonators (FBARs) and filters are a promising technology to fulfill this requirement in SHF range, offering high-quality factor (*Q*) and a large electromechanical coupling coefficient (k_t^2) [1], [2]. To scale up the resonant frequency of FBARs, the thickness of the piezoelectric material needs to be reduced to sub-micron ranges. However, crystallinity becomes a significant issue when the device thickness is thinned down below 1 um to achieve higher frequency operation. There is a strong correlation between the crystallinity of the piezoelectric layer and *Q*-factor, as well as the k_t^2 of the device, showing limited *Q* of polycrystalline thin films by an increase in the scattering losses at the grain boundaries of films and degraded k_t^2 dueto larger full width at half maximum (FWHM), showing poor crystallinity of thin-film [3], [4]. Furthermore, the metal electrodes are needed to be optimized for SHF operation. The electromechanical coupling coefficient of FBAR is highly dependent on the thickness ratio between metal and piezoelectric layers [5]. However, thining down the metal electrode is challenging since the sheet resistivity of the metal layer increases as the metal thickness decreases [6]. In addition, the crystallinity of the metal layer for the bottom electrodes plays an important role in supporting the formation of a well-oriented piezoelectric layer with surface uniformity [7]. Aluminum nitride (AlN) is popular in today's FBARs due to the well-developed micromachining techniques as well as relatively high phase velocity and large *Q* for high-frequency operation [7]. Scandium aluminum nitride (ScAlN) is recently introduced showing the enhanced electromechanical coupling coefficient by an increase in the piezoelectric coefficient up to 4-5 times larger than pure AlN [8], [9]. AlN/ScAlN are mostly deposited using sputtering techniques owing to low cost and relatively high growth rates [10]. However, polycrystalline AlN/ScAlN films show degraded crystal quality when the thickness of films is smaller than 1um [3], [4].

This work utilizes a novel all-crystalline epitaxial stack of metal/ScAlN grown on engineered oxide on Si substrate as shown in Fig.1. Due to the high quality of epitaxial thin metal and piezoelectric material growth, a high *Q* of 1230 is achieved for a 4.6 GHz fundamental thickness mode, yielding an $f \times Q$ value of 5.6×10^{12} Hz. Second and third-order overtone resonance modes are picked up at 11.8 and 19.0 GHz with $f \times Q$ value of 2.5×10^{12} Hz and 2.3×10^{12} Hz, respectively. This work is the first demonstration of a multi-GHz FBAR realized on single-crystalline 12% SCAlN/Mo stack.

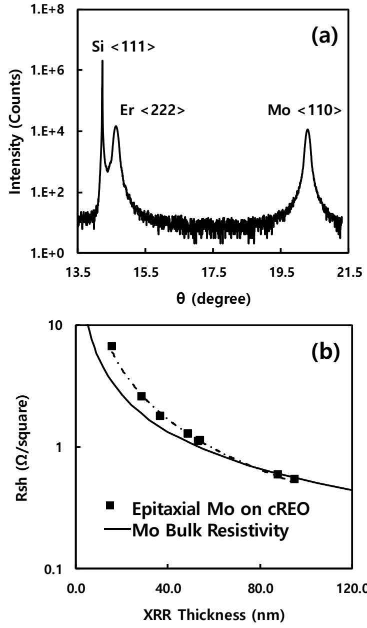

Fig.2. Material characterization: (a) X-ray diffraction (XRD) pattern for epitaxial Mo-cREO on Si (111) and (b) sheet resistivity of epitaxial Mo on cREO/Bulk Mo on Si, according to Mo thickness by using X-ray reflectivity (XRR) [8].

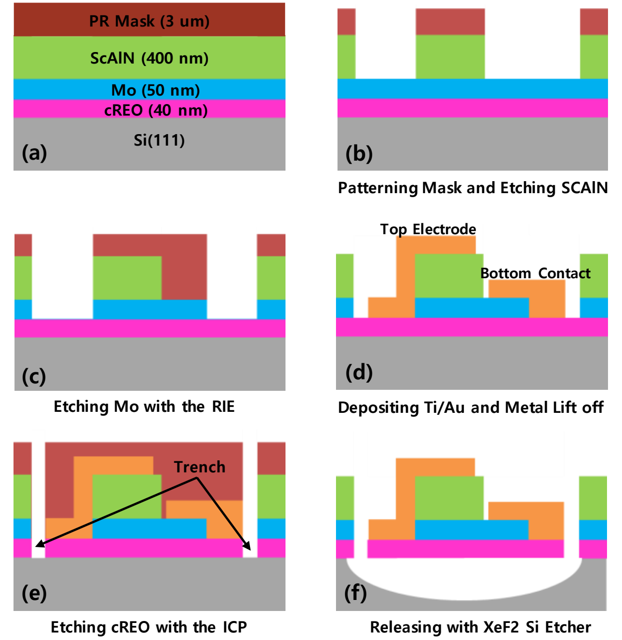

Fig.3. Sequencial steps of the fabrication process of the single-crystaline ScAlN FBAR: (a) single-crystalline ScAlN-Mo-cREO on Si (111); (b) etching ScAlN with PR mask patterned by MLA; (c) eching Mo with RIE; (d) deposting Ti/Au with a thickness of 5/75 nm for top and bottom electordes and metal lift off; (e) etching cREO with the plasmaPT-ICP for device trench; (f) releasing devices with XeF_2 Si etcher.

II. Thin Film Material Characteristics and Fabrication Process

A. *Thin Film Material Characteristics*

The thin-film single crystalline (12%) ScAlN with a thickness of 400 nm is directly grown on top of the epitaxial Molybdenum (Mo) with a thickness of 50 nm as the bottom electrode of the acoustic device by using molecular beam epitaxy (MBE) [6]. The epitaxially-grown Mo is thinned down to match the scaling of the device based on the thickness of the piezoelectric layer [5]. A crystal rare earth oxide (cREO) layer with a thickness of 40 nm is grown on top of the Si substrate to prevent the formation of a metal silicide as a chemical barrier between the metal layer and the underlying silicon [6]. The crystal structure of epitaxially grown Mo-cREO on Si was analyzed using an X-ray diffraction (XRD) pattern as shown in Fig.2(a) [6]. FWHM value in the range from 0.8 to 1˚ is scanned with the <110> rocking curve at θ = 20.31˚ for epitaxial Mo-cREO on Si. Fig.2(b) illustrates the sheet resistivity of epi-Mo on cREO depending on the X-ray reflectivity (XRR) thickness, showing that the measured sheet resistivity of epi-Mo-cREO has a similar trend compared to that of conventional bulk Mo. Furthermore, it is noted that epi-metal layers as thin as 40 nm can be successfully grown with < 20% deviation from the ideal metal [6].

B. *Fabrication Process*

The sequential steps of the microfabrication process are described in Fig.3. First, 3 µm thick of photoresist (PR) is used for etch mask and patterned by maskless aligner (MLA). 400 nm thick single-crystal ScAlN piezoelectric layer is etched by Cl_3-based thermal inductively coupled plasma (ICP) to expose the Mo metal layer as shown in Fig.3(a)-(b). Then, the 50 nm thick epitaxial Mo is patterned by the reactive ion etcher (RIE) plasma system to expose cREO layer as depicted in Fig.3(c). After cleaning the remaining PR mask, Ti/Au with a thickness of 5 /75 nm is deposited as the top electrode and lead to access the bottom electrode, as presented in Fig.3(d). As shown in Fig.3(e), the cREO is etched by ICP to access the Si substrate. Finally, the devices are released from the host Si substrate using xenon difluoride (XeF_2)-based isotropic Si etcher as shown in Fig.3(f). Fig.1 shows the scanning electron microscope (SEM) image of the apodized FBAR with one-port GSG pads with the overall cross-section of the resonator stack.

III. Device Characteristics and Experimental Results

A. *Characterization of Over-tone Resonance Modes*

Fig. 4(a) illustrates the COMSOL finite element analysis (FEA) simulation result of the excited thickness resonance modes along with the displacement of mode shapes with a stack of 12% ScAlN piezo-electric layer (400 nm-thick), Mo bottom electrode epi-metal layer (50 nm-thick), cREO layer (40 nm-thick) and Ti/Au top electrodes (5/75 nm-thick). The piezoelectric coefficients and elastic constants of $Sc_{0.12}Al_{0.88}N$ are estimated based on the Sc composition of ScAlN films [11], [12]. The fundamental thickness mode is induced at the resonant frequency of 4.6 GHz. The second and third-order resonance modes are picked up at resonant frequencies of 11.96 and 18.99 GHz. Fig.4(b) shows the measured wide-band response of the Y_{11} magnitude fitted with Mason's model at the frequency range from 1-20 GHz. Mason's model can be utilized for the FBAR device to characterize the electrical and

TABLE I. ELECTROMECHANICAL PARAMETERS EXTRACTED FROM MBVD MODEL FITTING OF SCALN FBAR RESONATOR.

	f_{res} (GHz)	f_s (GHz)	f_p (fF)	C_o (fF)	C_m (fF)	L_m (nH)	R_m (Ω)	Q_m	k_t^2 (%)	$f \times Q$ (Hz)	$f \times Q \times k_t^2$(GHz)
1st Mode	4.6	4.64	4.66	203	2.54	463	11	1230	1	5.6×10^{12}	56.55
2nd Mode	11.84	11.17	11.81	203	4.91	37.4	13	212	1.86	2.5×10^{12}	46.82
3rd Mode	19	18.8	19.1	203	7.59	9.3	9	123	3.56	2.3×10^{12}	83.28

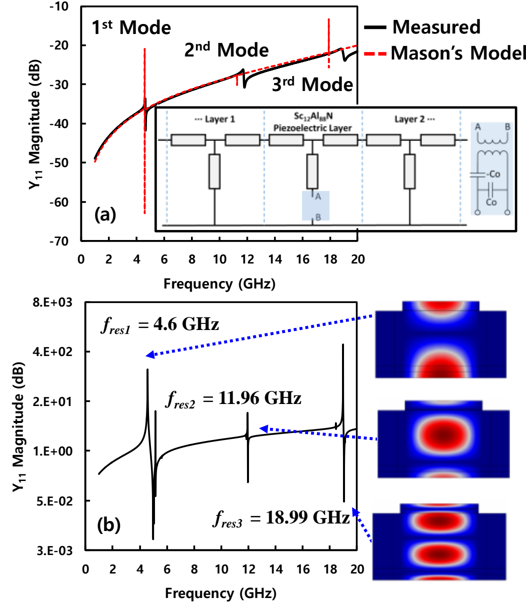

Fig.4. (a) Measurement results of wideband (1-20 GHz) frequency response of FBAR along with simulated frequency response from the Mason's model. (b) COMSOL simulation results of the wide-band frequency response of FBAR along with the corresponding over-tone displacement mode shapes, where blue and red denote the minimum and maximum displacement. The fundamental thickness mode at 4.6 GHz is observed along with Ku-band second and third-order modes at 11.96 GHz and 18.99 GHz. A thickness of 400 nm is used for ScAlN, 80 nm for the top electrode, 50 nm for the Mo and 40 nm for cREO.

mechanical components of the resonator by modeling each layer of the stack [13]. Each layer of the FBAR stack is evaluated using the acoustic velocity and impedance, which are defined based on the Young's modulus, mass density, and thickness of the material. The static capacitance (C_o) of the piezoelectric layer is determined by the permittivity and the dimension of the piezoelectric layer [14]. From Mason's model, the fundamental, second, and third-order resonance modes are excited at the resonant frequencies of 4.6, 11.28, and 17.91 GHz, wherein each of the resonant peaks is plotted together the correlated resonant frequency of the measured response in Fig. 4(a), wideband COMSOL frequency response along with the displacement mode shapes are shown in Fig. 4(b).

B. Frequency Response of FABR with MBVD Fitted Model

The device is tested using Keysight N54244B PNA microwave network analyzer. Fig.4(a) shows the wide-band magnitude of admittance (*Y*)-parameter, which is measured over a frequency range from 1 to 20 GHz. Fig.5(b)–(g) demonstrate the corresponding zoomed-in peaks of fundamental and overtone resonance modes showing Y_{11} magnitude and phase response of the scattering matrix (*S*)-parameters. The measured

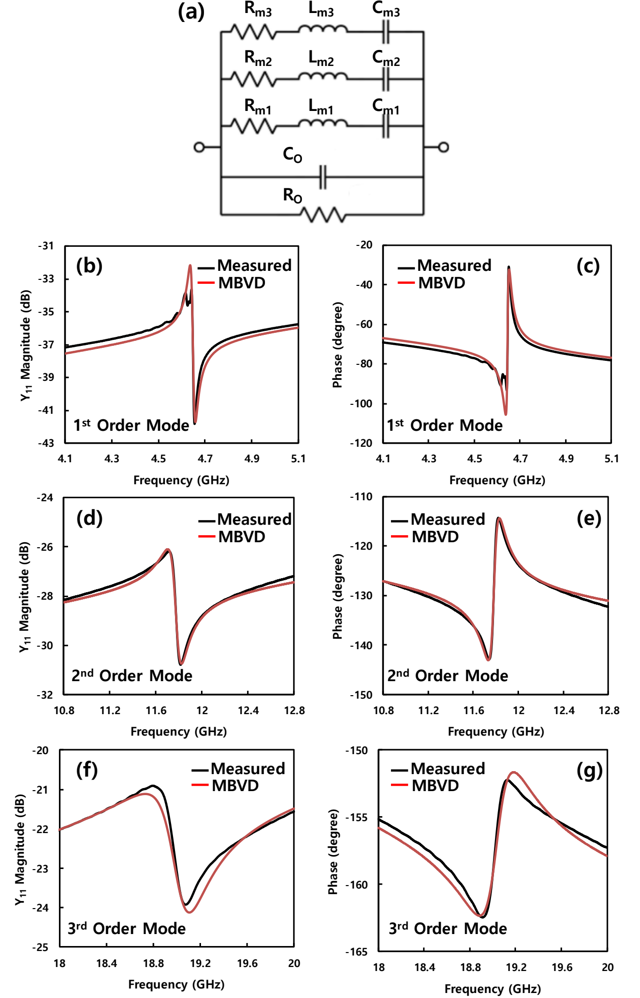

Fig.5. (a) : Characteristic of FBAR with Butterworth-Van Dyke (MBVD) model fitting with three motional branches. (b)-(g) : Measurement result of FBAR with characterizing resonance modes using MBVD model fitting. Zoomed-in measured admittance and phase response of fundamental: (b)-(c), 2nd order: (d)-(e) and 3rd order: (f)-(g) is fitted with MBVD model.

results are characterized by the Modified Butterworth-Van Dyke (MBVD) fitted model [15]. As shown in Fig.5(a), the model consists of the equivalent electrical components described with the static capacitor C_o and the parallel resistor R_o. R_m, L_m, and C_m depict the motional branches, including the fundamental, second and third-order resonance modes [15], sharing the same C_o and R_o. C_o and R_o are evaluated by using imaginary and real parts of the off-resonance of *Y*- and *Z*- parameters [11], [16]. The evaluated C_o and R_o are 203 fF and 1451 KΩ, respectively. The unloaded quality factor (Q_m) of the resonator is estimated using the motional branch as :

$$Q_m = \frac{1}{R_m}\sqrt{\frac{L_m}{C_m}}. \quad (1)$$

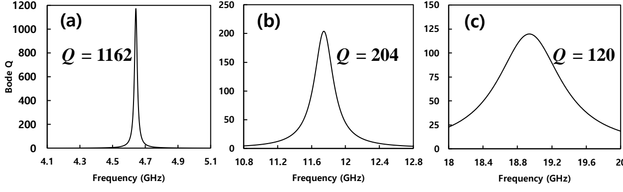

Fig.6. Extracted Bode Q of FBAR based on S_{11} with 50Ω source impedance matching: (a) fundamental resonance mode with bode Q_m of 1162, (b) second order resonance mode bode Q_m of 204, and (c) third order resonance mode Bode Q_m of 120.

Fig.5(b)–(c) show the excited fundamental thickness mode at the resonant frequency of 4.6 GHz. Fig.5(d)–(g) present higher-order resonance modes at the resonant frequency of 11.8 and 19 GHz. The highest Q_m is 1230 at 4.6 GHz.

Another method to compute Q based on S_{11} is using Bode Q. Here, we apply the Bode Q method to the motional branch of the S_{11} fitted MBVD curves using [17] :

$$Q_{bode} = \omega \times \frac{|S_{11}| group_delay(S_{11})}{1-|S_{11}|^2}. \quad (2)$$

The above expression for Q_{bode} is defined based on the phase group delay of S-parameter in radian. It is noted that Eq (2) is valid only if the continuous Q circle is placed in the center of the smith chart using 50 Ω source impedance matching [17]. Fig.6 shows the evaluated unloaded Q along with the frequency response achieving Q_{bode} of 1162 for (a) fundamental, 204 for (b) second- and 120 for (c) third-order thickness modes, which are equivalent to Q_m determined by the motional branch of the MBVD model fitting.

The effective electromechanical coupling coefficient (k_t^2) is extracted from [11], [18]:

$$k_t^2 = \frac{\pi^2}{4} \times \frac{f_s(f_p - f_s)}{f_p^2}. \quad (3)$$

Where f_s is the series and f_p is the parallel resonant frequency which is determined from measured admittance (Y_{11})-parameter of the device. The evaluated largest k_t^2 of FBAR is 3.56% at the resonant frequency of 19 GHz. Table I summarizes the MBVD parameters and evaluated Q_m of the FBAR.

IV. Conclusion

In this paper, single-crystalline 12% ScAlN films were investigated for the fabrication of the FBARs at a super high frequency range. We took advantage of the high crystal quality of ultra-thin ScAlN epi-layer. Moreover, we employed epitaxially-grown Molybdenum (Mo) as a bottom electrode and thinned down the metal thickness to 50 nm to match the scaling of the device. This work is the first demonstration of multi-GHz FBARs realized on single-crystalline ScAlN/Mo stack, yielding a very high $f \times Q$ value of 5.64×10^{12} Hz and $f \times Q \times k_t^2$ value of 8.33×10^{10} Hz as summarized in Table I.

Acknowledgment

This work is sponsored by the company IQE PLC, and the devices were fabricated at Georgia Institute of Technology for IEN cleanroom, a member of the National Nanotechnology Coordinated Infrastructure (NNCI), which is supported by the National Science Foundation (Grant ECCS-1542174).

References

[1] J. B. Shealy et al., “Low loss, 3.7GHz wideband BAW filters, using high power single crystal AlN-on-SiC resonators,” IEEE MTT-S Int. Microw. Symp. Dig., pp. 1476–1479, 2017.

[2] A. Ansari, “Single Crystalline Scandium Aluminum Nitride : An Emerging Material for 5G Acoustic Filters,” in *IEEE MTT-S International Microwave Symposium*, 2019, pp. 1–3.

[3] L. Shu *et al.*, “The characterization of surface acoustic wave devices based on AlN-metal structures,” *Sensors (Switzerland)*, vol. 16, no. 4, 2016.

[4] E. Yarar, V. Hrkac, C. Zamponi, A. Piorra, L. Kienle, and E. Quandt, “Low temperature aluminum nitride thin films for sensory applications,” *AIP Adv.*, vol. 6, no. 7, 2016.

[5] M. Hara *et al.*, “Super-high-frequency band filters configured with air-gap-type thin-film bulk acoustic resonators,” *Jpn. J. Appl. Phys.*, vol. 49, no. 7 PART 2, 2010.

[6] A. Clark *et al.*, “Epitaxial materials for RF filters,” *CS MANTECH 2019 - 2019 Int. Conf. Compd. Semicond. Manuf. Technol. Dig. Pap.*, pp. 10–12, 2019.

[7] Y. Yoshino, “Piezoelectric thin films and their applications for electronics,” *J. Appl. Phys.*, vol. 105, no. 6, 2009.

[8] M. Akiyama, T. Kamohara, K. Kano, A. Teshigahara, Y. Takeuchi, and N. Kawahara, “Enhancement of piezoelectric response in scandium aluminum nitride alloy thin films prepared by dual reactive cosputtering,” *Adv. Mater.*, vol. 21, no. 5, pp. 593–596, 2009.

[9] F. Martin, P. Muralt, M.-A. Dubois, and A. Pezous, “Thickness dependence of the properties of highly *c* -axis textured AlN thin films,” *J. Vac. Sci. Technol. A Vacuum, Surfaces, Film.*, vol. 22, no. 2, pp. 361–365, 2004.

[10] P. O. Å . Persson *et al.*, “ Microstructure and dielectric properties of piezoelectric magnetron sputtered w-Sc x Al 1−x N thin films ,” *J. Appl. Phys.*, vol. 111, no. 9, p. 093527, 2012.

[11] M. Park, Z. Hao, D. G. Kim, A. Clark, R. Dargis, and A. Ansari, “A 10 GHz Single Crystalline Sc-AlN Lamb-wave Resonator,” in *IEEE Transducers Conference 2019*, 2019.

[12] M. A. Caro *et al.*, “Erratum: Piezoelectric coefficients and spontaneous polarization of ScAlN (Journal of Physics: Condensed Matter (2015) 27 (245901)),” *J. Phys. Condens. Matter*, vol. 27, no. 27, 2015.

[13] T. Jamneala, P. Bradley, U. B. Koelle, and A. Chien, “Modified Mason Model for bulk acoustic wave resonators,” *IEEE Trans. Ultrason. Ferroelectr. Freq. Control*, vol. 55, no. 9, pp. 2025–2029, 2008.

[14] J. A. HAGLUND and O. HUNTER, “Elastic Properties of Polycrystalline Monoclinic Gd2O3,” *J. Am. Ceram. Soc.*, vol. 56, no. 6, pp. 327–330, 1973.

[15] R. Lu, M. H. Li, Y. Yang, T. Manzaneque, and S. Gong, “Accurate Extraction of Large Electromechanical Coupling in Piezoelectric MEMS Resonators,” *J. Microelectromechanical Syst.*, pp. 1–10, 2019.

[16] M. Park, Z. Hao, R. Dargis, A. Clark, and A. Ansari, “Super High Frequency Acoustic Resonators Based on Scandium Aluminum Nitride Crystalline Thin Films,” submitted for publication, 2019.

[17] D. A. Feld, R. Parker, R. Ruby, P. Bradley, and S. Dong, “After 60 years: A new formula for computing quality factor is warranted,” *Proc. - IEEE Ultrason. Symp.*, no. 6, pp. 431–436, 2008.

[18] Z. Hao *et al.*, “Single Crystalline ScAlN Surface Acoustic Wave Resonators with Large Figure of Merit (Q × k t2),” pp. 786–789, 2019.